ENGINEERING TRANSACTIONS • *Engng. Trans.* • **51**, 2-3, 195–214, 2003
Polish Academy of Sciences • Institute of Fundamental Technological Research
10.24423/engtrans.486.2003

INFLUENCE OF BONE ANISOTROPY ON STRESS DISTRIBUTION AND OPTIMUM SHAPE OF CEMENTLESS FEMORAL IMPLANTS

P. Kowalczyk

Institute of Fundamental Technological Research
Polish Academy of Sciences,
Świętokrzyska 21, 00-049 Warszawa, Poland
e-mail:pkowalcz@ippt.gov.pl

Implant separation from bone tissue, resulting in the necessity for revision surgery, is a serious drawback of cementless total joint replacement. Unnatural stress distribution around the implant is considered the main reason for the failure. Optimization of the implant properties, especially its geometric parameters, is believed to be the right way to improve reliability of joint prosthetics. Numerical models of femur–implant system enabling approximate analysis of stress distribution and shape optimization of implants suffer from numerous simplifications as, e.g., the assumption of bone isotropy, which may put in question reliability of the results obtained. In this paper, a numerical model including orthotropic properties of both cancellous and cortical bone is presented and influence of this assumption on results of the analysis and optimization is investigated.

1. Introduction

Total joint replacement is a standard surgical technique employed in treatment of various types of joint diseases and damages, especially in hips and knees. The surgery consists in removal of femoral head and acetabular surface and placement of a pair of implants, being elements of an artificial joint, in cavities of appropriately drilled bones. Implants can either be directly forced (press-fitted) into the cavity or fixed to its walls by an interfacing layer of flexible polymeric cement (like PMMA). In the present paper, prostheses of the first (cementless) type are only considered.

This technique has, however, a number of drawbacks. Long-term and short-term aseptic loosening of artificial joint components in bones belong to the most serious of them. The first one occurs typically 10–20 years after

surgery [15]. The precise mechanism of the failure is not clear, however, mechanical rather than medical factors are reported to play the major role. In cementless implants, load transfer between a stiff implant and relatively flexible bone results in extremely unnatural stress distribution in the latter, i.e. excessive stress concentrations near to the implant ends, and stress shielding [5, 14] followed by bone resorption in other areas of the bone–implant interface. The reason for short-term loosening are relative micromotions resulting, e.g., from improper implant fitting in the bone cavity. These may affect bone ingrowth into the porous implant surface and, consequently, lead to permanent debonding of implant from bone, HUISKES and VERDONSCHOT [15] and references cited therein.

Stresses and motions in bone and implant depend mainly on loading conditions and on the implant design, i.e. its mechanical properties and geometry. As the latter is easy to be modified in quite a wide range, design optimization of the implant shape appears to be a promising way to improve the reliability of joint prosthetics.

Numerical simulations of mechanical behavior of bone–implant systems are mainly based on the finite element method [34]. PRENDERGAST reports in his review paper [23] over two hundred contributions in this field. The method is criticized for limited reliability of results due to effects of mesh size and distortion, simplified constitutive models and loading conditions. Yet, it still remains the fundamental non-invasive tool in effective analysing of deformation and stress distribution in both intact and implanted bones.

Design optimization of implants requires, apart from the numerical analysis tool, the computation of design gradients (sensitivity) and an efficient optimum search algorithm. Publications on design sensitivity of implants appeared in the literature since early 80's [32] but it is only in recent years that comprehensive finite-element sensitivity and optimization studies have become of major interest of researchers, e.g. [3, 10, 11, 13, 20]. In these studies, one- and two-dimensional models of bone–implant interaction were analysed with optimization of the implant shape or mechanical properties. Such models enable efficient analysis, but they fail to include fully 3-D effects which is a serious drawback. An example of a 3-D analysis and optimization of the femoral implant shape can be found in [18]. However, even in the latter paper, bone is assumed to be isotropically elastic which again raises a question of reliability of the results.

The objective of this paper is to compare the earlier numerical results [18] with the results of analogous analysis performed under the assumption of anisotropic properties of bone. The parametric transversely isotropic bone model based on numerical analysis of equivalent microstructure [19] has been employed.

2. Physical and numerical model

2.1. Geometry and load

The geometry and loading conditions of the model are assumed identical as in [18]. Figure 2.1 displays the frontal cross-section of the 3-dimensional model of a femur with the hip endoprosthesis. The geometry of bone is simplified in the sense that the planar symmetry with respect to the frontal mid-plane is assumed, for both bone and implant. This simplification is not expected to significantly affect the stress distribution in bone; on the other hand it enables easy automatic generation of finite element meshes of the system for different values of implant shape parameters.

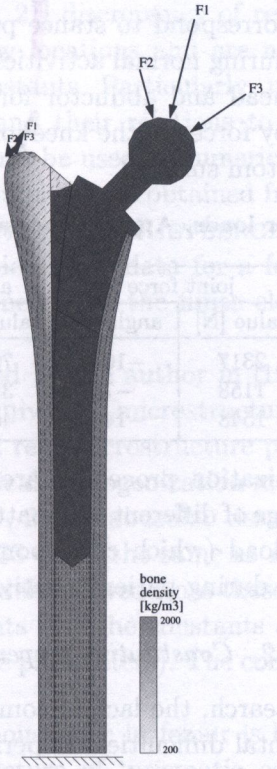

Fig. 1. Physical model. The winglet base line and the boundary of the proximal porous coated area on the implant surface, are marked in the implant cross-section. Short lines in the bone cross-section denote principal directions of orthotropy.

A standard implant with oval cross-section, bent shape and a vertical stabilizing "winglet" on the lateral side is considered (see Sec. 2.3 for more details of the bone and implant transversal cross-sections). The upper part of the im-

plant surface is porous-coated to induce tissue ingrowth and better adhesion between bone and implant. The lower boundary of the coated area is marked with a skewed line in Fig. 2.1. The remaining part of the implant surface is assumed smooth. In the computations, low-friction contact is assumed on the smooth bone–implant interface (in fact, since little is known about the value of the friction coefficient, it is taken as zero). The porous-coated interface is modelled as the high-friction interface which, under certain assumptions discussed in Section 3.2, can be simplified to the perfect bonding contact condition.

Load conditions have strong influence on the stress distribution and, consequently, on the result of shape optimization. The hip joint is subjected to various types of loads in the patient's everyday life activities (walking, running, standing, etc.). The three loading cases shown in Fig. 2.1 are equal to loads analysed by CARTER *et al.* [2] and correspond to stance phase of gait (F_1) and two extreme situations occurring during normal activities (F_2 and F_3). The load values and angles for both joint head and abductor forces are displayed in Table 1. The loads are equilibrated by forces in the knee joint (replaced by the boundary condition on the cut-off bottom surface).

Table 1. Numerical data for loads. Angle is measured from the horizontal axis.

Load case	joint force		abductor force	
	value [N]	angle [°]	value [N]	angle [°]
1	2317	−104	702	62
2	1158	−75	351	98
3	1548	−146	469	55

The analysis and optimization procedure are performed for an equivalent load, being a weighted average of different load patterns. Following [2], we assume the same weights for each load (which corresponds to equal number of cycles occurring for each load case during patient's activities).

2.2. Constitutive properties

In the biomechanical research, the lack of comprehensive and reliable material data is one of fundamental difficulties. Experimental studies, especially for cancellous bone, give results that are fragmentary and prone to various types of errors. They do not provide sufficient information necessary to perform computations, i.e., in the general case, nine orthotropic elastic constants plus three angles describing orientation of principal directions of orthotropy (in the case of transverse isotropy this reduces to five elastic constants and two angles). Additionally, due to the material inhomogeneity, all these constitutive parameters must be understood as function of spatial location – we thus do not need just their values, but spatial distributions.

Cortical bone is probably the most easy tissue to investigate experimentally and thus best documented in the literature. Yet, even in this case, the results reported differ much from each other depending on the source [4]. In the following analysis, cortical bone is treated as transversely isotropic material with the principal axis of the higher stiffness modulus E_3 oriented longitudinally and tangentially to the bone surface. Elastic constants are taken as average of results obtained in [1, 24, 33] and are assumed as follows:

$$\begin{aligned} E_1 &= E_2 = 14.33 \text{ GPa}, & E_3 &= 21.5 \text{ GPa}, \\ \nu_{12} &= 0.43, & \nu_{31} &= \nu_{32} = 0.367, \\ G_{12} &= 5.0 \text{ GPa}, & G_{31} &= G_{32} = 5.95 \text{ GPa}. \end{aligned}$$

For cancellous bone [8, 9, 12, 21] discrepancy of results is even larger, besides, data are acquired at only few locations and are not complete in the sense of number of the measured constants. Particularly, nothing is known about the directions of principal axes and their relations to directions of the measured moduli. Thus, such data cannot be used in numerical analysis.

Much more exhaustive results can be obtained from the numerical investigations of trabecular microstructure. VAN RIETBERGEN and coworkers [26, 27, 31] report a set of full orthotropic elastic data for a few hundreds of human cancellous bone specimens obtained from the finite element analysis of micro-CT scans.

Another method, employed by the author in [19], consists in finite element analysis of parameterized equivalent microstructures consisting of repeatable cells corresponding to typical real microstructure patterns. This is a numerical counterpart to the mathematical homogenization methods developed for trabecular microstructures e.g. in [7, 29]. Trabecular tissue is assumed isotropic, with the elastic constants $E = 14.33$ GPa (the same as E_1 for cortical bone, cf. [30]) and $\nu = 0.3$. Constitutive models derived from these data have the advantage of parameterized elastic constants (i.e. the constants are given as tabulated functions of certain microstructure parameters). The constitutive models of this type will be used in this paper.

It is assumed that cancellous bone in femur is built of interconnecting bars only, and forms a microstructure of 'prismatic cells' (using the terminology of [19]), i.e. each microstructural node is a 5-bar node. This yields microstructures with the macroscopic properties of transverse isotropy with remarkably higher stiffness in the principal direction. Within the range of volume fraction between 0.1 and 0.3 the ratio E_3/E_1 varies from about 2.5 to 1.5. Since this microstructure is parameterized by only one parameter (bar thickness), we can as well parameterize it by volume fraction instead. Thus, to define material properties of cancellous bone, it is necessary to provide distribution of volume

fraction within the bone and distribution of orientation of principal direction of anisotropy.

There is no precise recipe to define the distributions. The only way to provide this information to the numerical model seems to do it in an arbitrary way based on visual examination of femur cross-sections. It is known from experimental studies [12] that the cancellous bone density in the proximal femur (excluding head) takes values from 200 to 300 g/cm^2 which corresponds to volume fractions of 0.1 to 0.15. From anatomical cross-sections it can be seen that the orientation angle of the microstructure characteristic direction is about 45° from the vertical axis. It can also be seen that trabeculae are somewhat more dense in the neighborhood of cortical bone and that the orientation angle is lower in this area.

Based on these observation, the distributions of volume fraction and of the orientation angles have been assumed in the form shown by short lines in Fig. 2.1. Values of anisotropic material constants at each location are found for a given volume fraction value from the tabulated data available from [19].

To compare the results obtained with the use of anisotropic constitutive models with results obtained for isotropic model, an equivalent distribution of isotropic elastic modulus E and Poisson ratio ν is introduced. In order to make the two models comparable to each other, the isotropic constants at each location are computed from the anisotropic values with the use of the least square methods. Minimized is the difference between five independent transversely isotropic coefficients of the stiffness matrix C_{11}, C_{33}, C_{12}, C_{13} and C_{66} computed from elastic constants of the anisotropic model, and their corresponding isotropic counterparts $\overline{C}_{11} = \overline{C}_{33} = \dfrac{E(1-\nu)}{(1+\nu)(1-2\nu)}$, $\overline{C}_{12} = \overline{C}_{13} = \dfrac{E\nu}{(1+\nu)(1-2\nu)}$, and $\overline{C}_{66} = \dfrac{E}{2(1+\nu)}$. The so obtained values of E and ν (for each location separately) are then used in the isotropic model.

DING [6] reported changes in cancellous bone density and stiffness with age. It is shown that in young subjects, before the age of 40 years, the stiffness modulus of cancellous bone increases at approximately constant volume fraction (which indicates tissue strengthening associated with increase of the microscopic stiffness modulus) while later, after the age of 50, both the stiffness modulus and the volume fraction decrease (which indicates that trabeculae get thinner at approximately constant tissue modulus). In order to evaluate how the phenomena affect the optimized implant shape, additional two numerical tests are performed. In one of them, all orthotropic elastic moduli of both trabecular and cortical tissue are diminished by 10%. In the other – density distribution is modified such that in most parts of cancellous bone the trabecular thickness is lower by about 5% (so that the overall macroscopic stiffness decreases by about

10%) and the thickness of cortical wall in the bone shaft is also diminished by 5%.

Material data taken for implant (titanium) in all numerical tests are: $E = 110$ GPa and $\nu = 0.33$.

2.3. Finite element discretization

The finite element discretization is shown in Fig. 2. The mesh basically consists of linear 8-node brick elements, but occasional prismatic, tetrahedral, and other types of degenerated linear continuum elements appear in the mesh as well. The contact layer is modelled with 8-node contact elements [17].

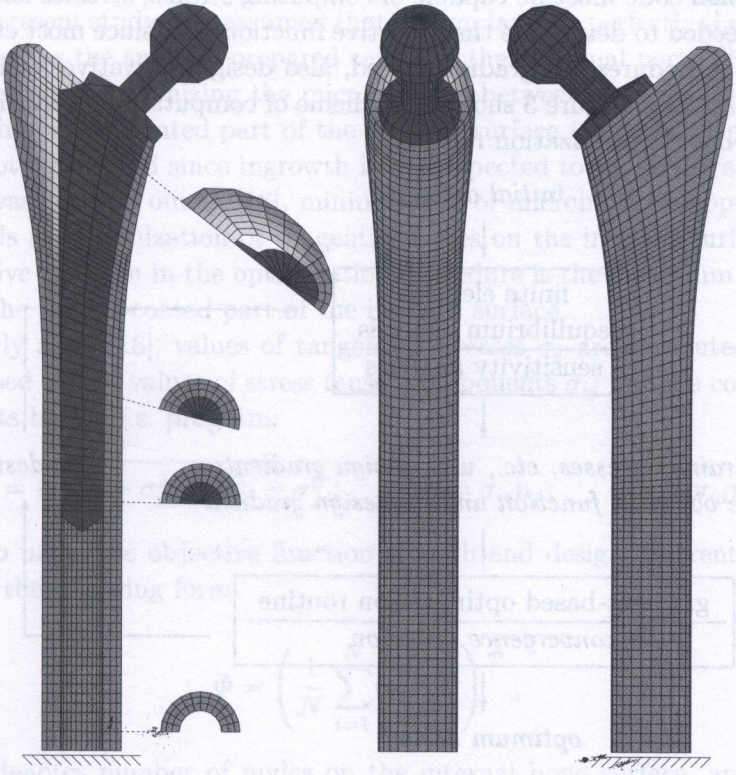

FIG. 2. Finite element model.

The mesh is obtained from a structured mesh generator written for this purpose. It allows for generation of meshes for different sets of implant shape parameters. The mesh topology (number of rows, circumferential segments, radial layers in each segment, etc.) is determined depending on the geometric proportions of implant and bone in the particular design, but it can as well be adopted

from another design, so that meshes with identical topology can be created for different design parameter sets.

3. Analysis and optimization

3.1. *Finite element procedure*

Numerical optimization of a mechanical system, like that consisting of bone and implant, requires the parameterized physical model of the system, a numerical code for static analysis, and an appropriate optimization scheme. The computational code must be capable of computing strains, stresses and all other variables needed to determine the objective function and, since most efficient optimization procedures are gradient-based, also design derivatives (sensitivities) of these quantities. Figure 3 shows the scheme of computations performed in the sensitivity-based optimization routine.

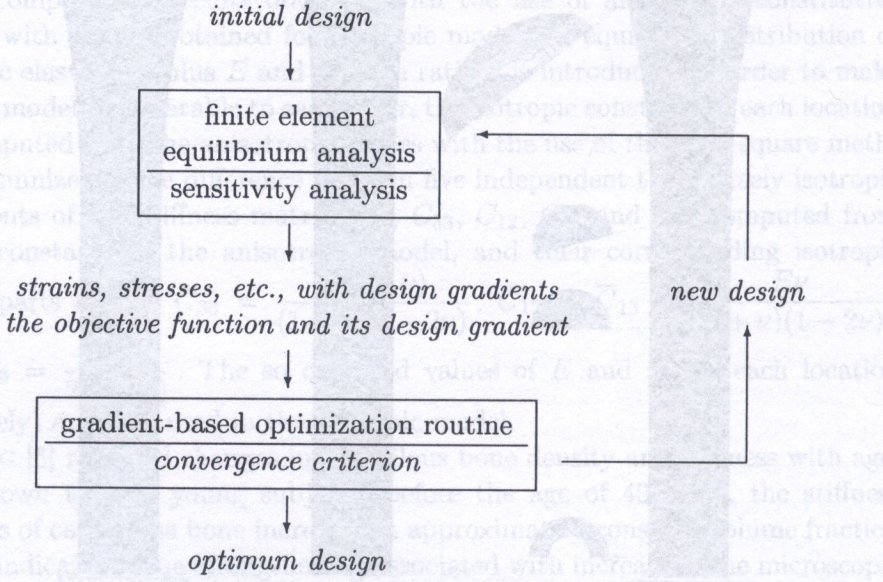

Fig. 3. Computation scheme in the optimization routine.

A finite element analysis code with the design sensitivity gradient computation routines implemented has been used. The program has been developed by the author at IFTR in Warsaw. Mathematical details of computational sensitivity analysis are presented in [16], and for the particular purpose of this type of biomechanical problems, in [18].

3.2. Optimization objective

The goal of optimization is to minimize the mechanical phenomena that are believed to result in the implant loosening. In this paper, short-term (post-operative) factors will be focused on. This failure type consists in improper bone ingrowth into the porous-coated implant surface which results in formation of permanent gaps filled with loose fibrous tissue. The reason for this may be either initial improper fitting of the implant into the medullary canal or excessive micromotions occurring at the bone–implant interface. Such micromotions can prevent osseointegration and a permanent layer of fibrous tissue is formed instead of the desired stiff bonding [15, 22]. Such a layer, even if mechanically stable, may lead in the long run to inflammatory reactions and bone resorption.

In the present study, it is assumed that the implant fits perfectly the medullary canal as well as the surgeon-prepared cavity in the proximal part. Thus, we are only interested in minimizing the micromotions between the bone internal surface and the porous-coated part of the implant surface (the smooth part of the latter is not considered since ingrowth is not expected to occur there, anyway).

As it was pointed out in [18], minimization of micromotions approximately corresponds to minimization of tangential forces on the implant surface. Thus, the objective function in the optimization procedure is the maximum tangential stress on the porous-coated part of the implant surface.

Similarly as in [18], values of tangential stresses $\sigma_{\|}$ are computed at nodal points, based on the values of stress tensor components σ_{ij} in bone computed at these points by the f.e. program:

$$\sigma_{\|} = \sqrt{\sigma_{\mathrm{n}1}^2 + \sigma_{\mathrm{n}2}^2 + \sigma_{\mathrm{n}3}^2 - \sigma_{\perp}^2}\,; \qquad \sigma_{\mathrm{n}i} = \sigma_{ij} n_j\,; \qquad \sigma_{\perp} = \sigma_{\mathrm{n}i} n_i\,.$$

In order to make the objective function smooth and design differentiable, it is written in the following form

$$\Phi = \left(\frac{1}{N} \sum_{i=1}^{N} (\sigma_{\|}^{(i)})^m \right)^{\frac{1}{m}},$$

where N denotes number of nodes on the internal bone surface, and m is an exponent. For m large enough,

$$\Phi \approx \max_{i=1,\ldots,N} \sigma_{\|}^{(i)}\,.$$

In this study, the following value for m is assumed,

$$m = \frac{\log N}{\log 1.02}\,.$$

3.3. *Design parameters*

The design parameters are shown in Fig. 4. These are: (1) the implant length, (2) the length of the porous-coated zone, (3) the height at which the lateral stem contour becomes curved, and (4) the depth of the lateral winglet corner. All parameters are 'non-dimensionalized', i.e. expressed as fractions of the bone shaft diameter (0.03 m) In the initial design (cf. geometry in Figs. 2.1, 4), the following values of design parameters have been chosen,

$$
\begin{aligned}
h_1 &= 5.0 \quad && (l = 150 \text{ mm}),\\
h_2 &= 1.666667 \quad && (l_r = 50 \text{ mm}),\\
h_3 &= 3.0 \quad && (l_l = 90 \text{ mm}),\\
h_4 &= 0.266667 \quad && (l_w = 8 \text{ mm}).
\end{aligned}
$$

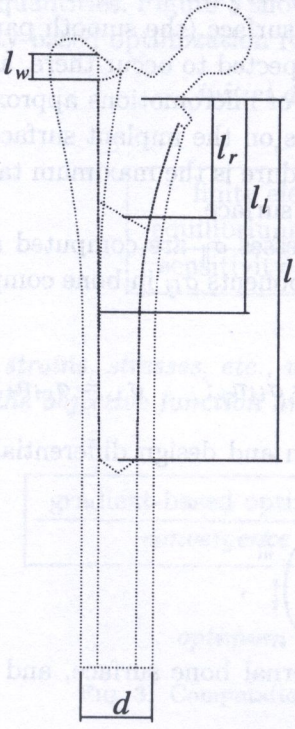

$h_1 = l/d$ – implant length

$h_2 = l_r/d$ – coated zone length

$h_3 = l_l/d$ – length of lateral curved contour

$h_4 = l_w/d$ – winglet corner depth

$d = 0.03\,\text{m}$ – bone shaft external diameter

FIG. 4. Definition of dimensionless design parameters.

3.4. *Optimization procedure*

Having the solution of the static problem, we can compute the current value of Φ; having the solution of the sensitivity problem, we can also easily com-

pute $d\Phi/d\mathbf{h}$. These quantities are necessary in any gradient-based optimization scheme. Here, the optimization procedure NLPQL described by SCHITTKOWSKI [28] is applied.

In each optimization task, the move limits (i.e. maximum values of design parameter variation) are set to $\pm 10\%$ of the parameters' current values, and the optimization is performed for the model with unchanged mesh topology according to the scheme in Fig. 3. When converged, i.e. when either the move limit is achieved or the design derivative does not exceed 0.01, the new mesh is generated for the computed optimum geometry and the procedure is repeated. The 10% limit is subsequently decreased as the final solution is approached (this setting is controlled manually). We must be aware of the fact that the objective function and its design derivatives may take slightly different values for different finite element meshes and thus the optimum for the new mesh topology may be different from the optimum found for the old one. Thus, final convergence is approved when: i) global minimum is found within the parameter move limits (all design derivatives < 0.01) for a certain mesh topology and ii) the new optimum mesh generated for this optimum geometry has the same topology as the old one.

4. RESULTS

Two computational tests have been performed. In the first test, an isotropic averaged constitutive model has been assumed at each location in compact and cancellous bone while in the second test the analogous transversely isotropic model with an appropriate distribution of principal orthotropic directions has been considered. In both tests, the same distribution of local density (volume fraction) in cancellous bone has been assumed (cf. Fig. 2.1) and the averaging procedure described in Sec. 2.2 was applied to ensure that the isotropic material constants in the first test correspond to the anisotropic ones in the second test.

4.1. Isotropic model

Figure 5 presents the computed stress distribution in bone at the bone–implant interface for the initial geometry model. Tangential stress on the medial and lateral side is displayed along the symmetric cross-section line (marked with a solid line in the bone contour in the figure center). Stresses presented in the graphs are limited to the porous-coated implant zone being of our interest. Stress concentrations are visible especially on the medial side at both ends of the porous-coated area. Figure 5 also displays the stress sensitivity graphs with respect to the four considered design parameters, along the same contour lines for the initial design.

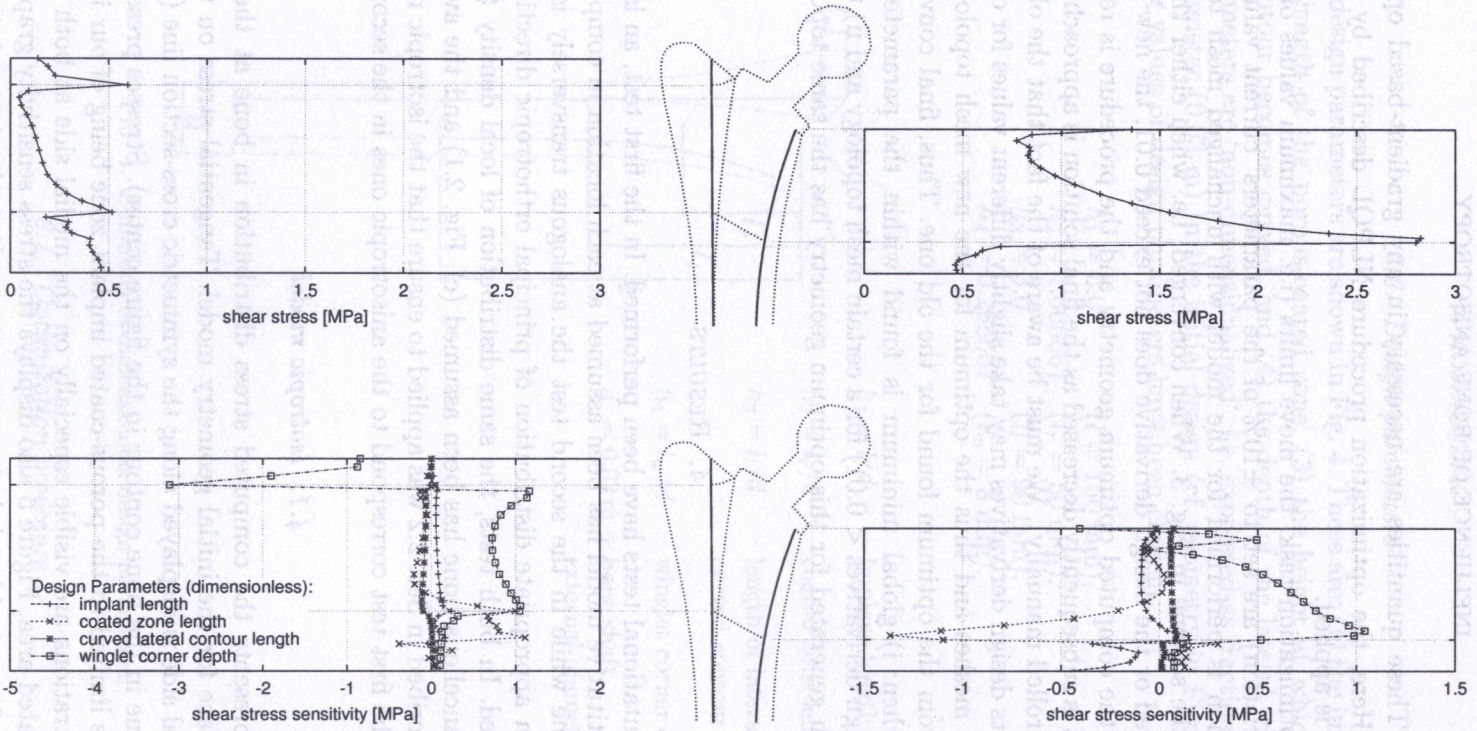

[206]

FIG. 5. Distributions of tangential stress (top) and its sensitivities (bottom) in bone along its internal surface on the lateral (left) and medial (right) side, for the isotropic model and for the initial implant design (as the design parameters are dimensionless, sensitivity has the stress units)

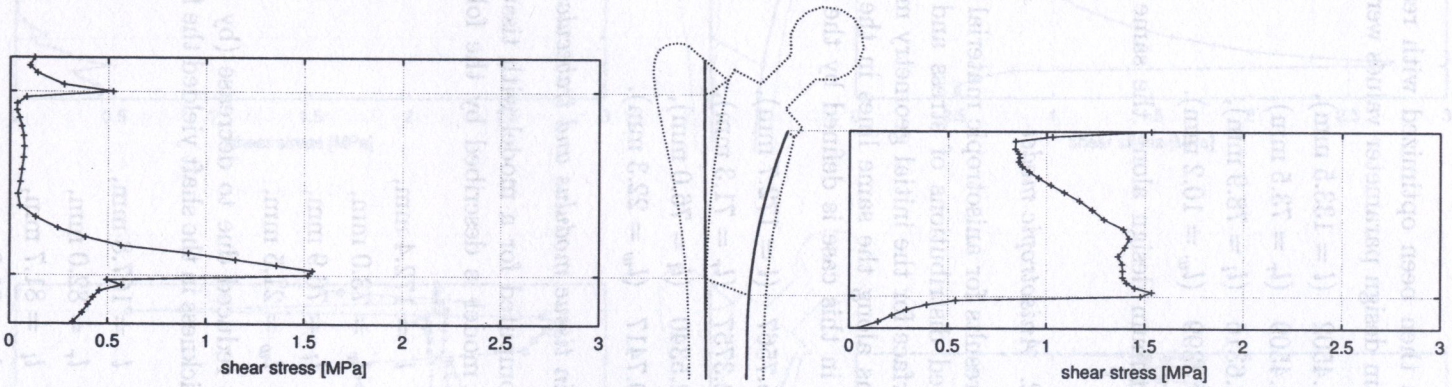

FIG. 6. Optimum tangential stress distribution in bone along its internal surface on the lateral (left) and medial (right) side, for the isotropic model.

This implant geometry has then been optimized with respect to the four design parameters. The optimum design parameter values were obtained as

$$h_1 = 4.4502 \quad (l = 133.5 \text{ mm}),$$
$$h_2 = 2.4509 \quad (l_r = 73.5 \text{ mm}),$$
$$h_3 = 2.6316 \quad (l_l = 78.9 \text{ mm}),$$
$$h_4 = 0.3399 \quad (l_w = 10.2 \text{ mm}).$$

Stress distributions for the optimum design along the same lines as those in Fig. 5 are presented in Fig. 6.

4.2. Anisotropic model

In Figs. 7 and 8 analogous results for anisotropic material model are shown. Figure 7 presents the computed distributions of stress and its sensitivity in bone at the bone–implant interface for the initial geometry model, while Fig. 8 presents the stress distributions along the same lines in the case of the optimum implant geometry which in this case is defined by the design parameter values

$$h_1 = 5.7567 \quad (l = 172.7 \text{ mm}),$$
$$h_2 = 2.3757 \quad (l_r = 71.3 \text{ mm}),$$
$$h_3 = 2.5340 \quad (l_l = 76.0 \text{ mm}),$$
$$h_4 = 0.7417 \quad (l_w = 22.3 \text{ mm}).$$

4.3. Effect of changes in tissue modulus and trabecular thickness

Optimum implant shape computed for a model with tissue elastic stiffness reduced by 10% in the entire model is described by the following parameter values,

$$l = 172.4 \text{ mm},$$
$$l_r = 73.0 \text{ mm},$$
$$l_l = 76.9 \text{ mm},$$
$$l_w = 21.5 \text{ mm}.$$

A model with overall stiffness reduced due to decrease (by 5%) of trabecular thicknesses and cortical wall thickness in the shaft yielded the following optimum shape parameters,

$$l = 167.8 \text{ mm},$$
$$l_r = 82.0 \text{ mm},$$
$$l_l = 81.7 \text{ mm},$$
$$l_w = 21.8 \text{ mm}.$$

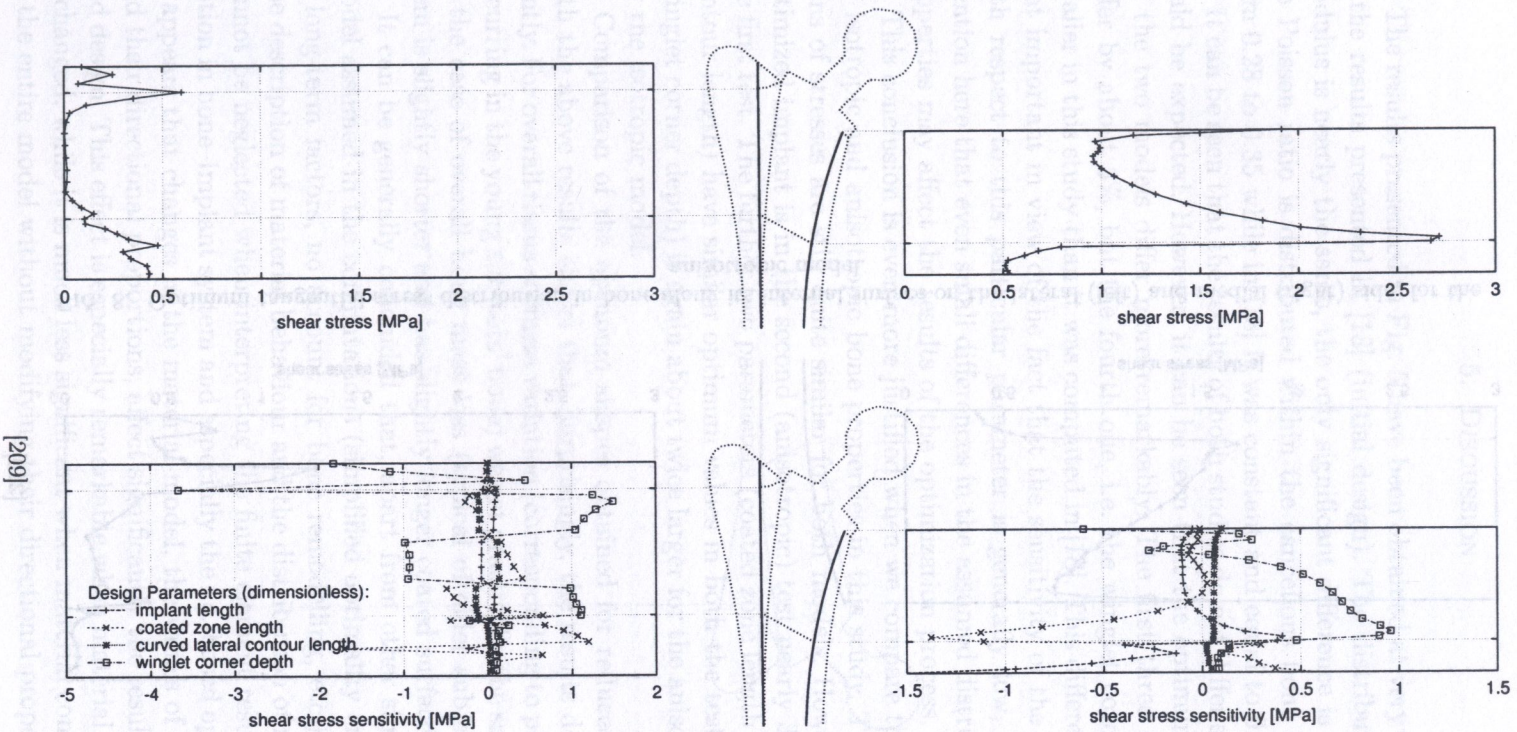

[209]

FIG. 7. Distributions of tangential stress (top) and its sensitivities (bottom) in bone along its internal surface on the lateral (left) and medial (right) side, for the anisotropic model and for the initial implant design (as the design parameters are dimensionless, sensitivity has the stress units).

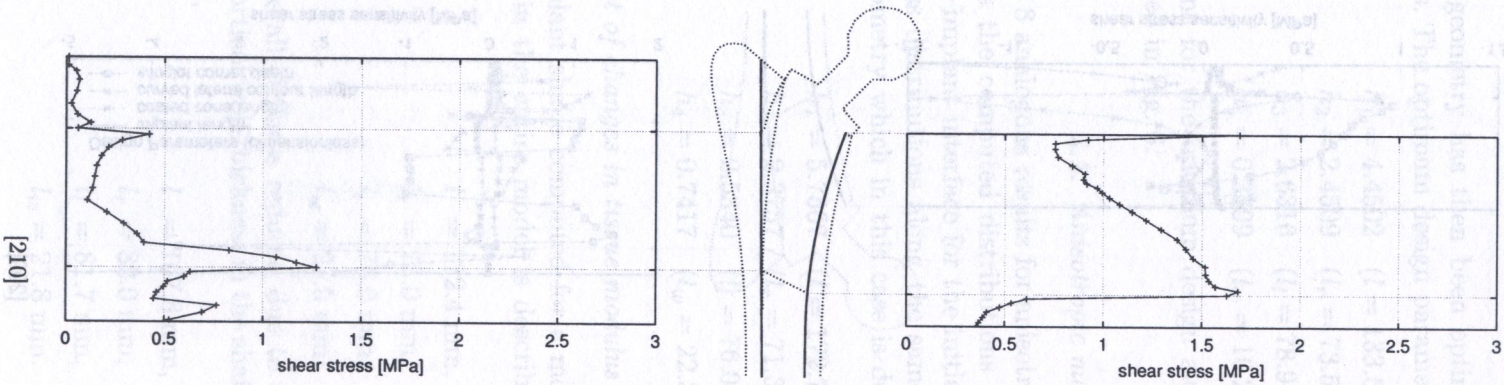

FIG. 8. Optimum tangential stress distribution in bone along its internal surface on the lateral (left) and medial (right) side, for the anisotropic model.

5. Discussion

The results presented in Fig. 5 have been obtained at very similar input data as the results presented in [18] (initial design). The distribution of the Young modulus is nearly the same, the only significant difference is that in this study the Poisson ratio is distributed within the cancellous bone and taking values from 0.28 to 0.35 while in [18] it was constant and equal to 0.35.

It can be seen that the results of both studies do not differ significantly, which could be expected. However, it can be seen that the optimum shapes obtained for the two models differ more remarkably. The first three design parameters differ by about 5%, but the fourth one, i.e. the winglet corner depth, is twice smaller in this study than it was computed in [18]. This difference is perhaps not that important in view of the fact that the sensitivity of the objective function with respect to this particular parameter is generally low, but still we must mention here that even small differences in the assumed distribution of material properties may affect the results of the optimization process.

This conclusion is even more justified when we compare the results obtained for isotropic and anisotropic bone properties in this study. The initial distributions of stresses are still quite similar for both models. However, the resulting optimized implant is in the second (anisotropic) test nearly 30% longer than in the first test. The further two parameters (coated zone length and curved lateral contour length) have similar optimum values in both the tests, while the latter (winglet corner depth) is again about twice larger for the anisotropic model than for the isotropic model.

Comparison of the optimum shapes obtained for reduced stiffness of bone with the above results shows that, surprisingly, the results do not differ significantly. For overall tissue stiffness variation (corresponding to physical phenomena occurring in the young subjects' bone) we get practically the same implant shape. In the case of overall bone mass loss (typical of older subjects), the optimum stem is slightly shorter and has slightly longer coated surface zone.

It can be generally concluded that, apart from other simplifications of the model assumed in the computations (simplified optimality criterion, negligence of long-term factors, no account for bone remodelling, etc.), the issue of precise description of material behaviour and the distribution of material properties cannot be neglected when interpreting the finite element results of stress distribution in bone–implant system and especially the f.e.-based optimization results. It appears that changes in the material model, the values of material constants and their directional proportions, affect significantly the results of computations and design. This effect is especially remarkable when material anisotropy of bone is changed, while it is much less significant when material constants are changed in the entire model without modifying their directional proportions.

Acknowledgment

Financial support from the Polish Committee for Scientific Research (KBN), grant no. 8 T11F 017 18, is gratefully acknowledged.

References

1. R. B. Ashman, S. C. Cowin, W. C. van Buskirk, J. C. Rice, *A continuous wave technique for the measurement for the elastic properties of bone*, Journal of Biomechanics, **17**, 349–361, 1984.
2. D. R. Carter, T. E. Orr, D. P. Fyhrie, *Relationships between loading history and femoral cancellous bone architecture*, Journal of Biomechanics, **22**, 231–244, 1989.
3. P. B. Chang, B. J. Williams, T. J. Santner, W. I. Notz, D. L. Bartel, *Robust optimization of total joint replacements incorporating environmental variables*, Transactions of the ASME, Journal of Biomechanical Engineering, **121**, 304–310, 1999.
4. Cowin S.C. [Ed.], *Bone mechanics*, CRC Press, 1989.
5. L. Cristofolini, *A critical analysis of stress-shielding evaluation of hip prostheses*, Critical Reviews in Biomedical Engineering, **25**, 409–483, 1997.
6. M. Ding, *Age variations in the properties of human tibial trabecular bone and cartilage*, Ph.D. Thesis, University of Aarhus, Denmark, 1999.
7. A. Gałka, J. J. Telega, S. Tokarzewski, *Application of homogenization to evaluation of effective moduli of linear elastic trabecular bone with plate-like structure*, Archives of Mechanics, **51**, 335–355, 1999.
8. E. B. W. Giesen, M. Ding, M. Dalstra, T. M. G. J. van Eijden, *Mechanical properties of cancellous bone in the human mandibular condyle are anisotropic*, Journal of Biomechanics, **34**, 799–803, 2001.
9. S. A. Goldstein, D. L. Wilson, D. A. Sonstegard, L. S. Matthews, *The mechanical properties of human tibial trabecular bone as a function of metaphyseal location*, Journal of Biomechanics, **16**, 965–969, 1983.
10. H. S. Hedia, D. C. Barton, J. Fisher, A. Ibrahim, *Shape optimisation of a Charnley prosthesis based on the fatigue notch factor*, Bio-Medical Materials and Engineering, **6**, 199–217, 1996.
11. H. S. Hedia, D. C. Barton, J. Fisher, *Material optimisation of the femoral component of a hip prosthesis based on the fatigue notch factor approach*, Bio-Medical Materials and Engineering, **7**, 83–98, 1997.
12. M.-C. Hobatho, J. Y. Rho, R. B. Ashman, *Anatomical variation of human cancellous bone mechanical properties in vitro*, [in:] Bone Research in Biomechanics, G. Lowet *et al.*, [Eds.], IOS Press, 1997.
13. R. Huiskes, R. Boeklagen, *Mathematical shape optimization of hip prosthesis design*, Journal of Biomechanics, **22**, 793–804, 1989.
14. R. Huiskes, H. Weinans, B. van Rietbergen, *The relationship between stress shielding and bone resorption around total hip stems and the effects of flexible materials*, Clinical Orthopaedics and Related Research, **274**, 124–134, 1992.

15. R. HUISKES, N. VERDONSCHOT, *Biomechanics of artificial joints: the hip.* [in:] V. C. MOW, W. C. HAYES [Eds.], Basic Orthopaedic Biomechanics, 2nd [ed.], pp. 395–460, Lippincott–Raven, Philadelphia, 1997.

16. M. KLEIBER, H. ANTÚNEZ, T. D. HIEN, P. KOWALCZYK, *Parameter sensitivity in nonlinear mechanics*, Wiley, Chichester, 1997.

17. P. KOWALCZYK, *Finite-deformation interface formulation for frictionless contact problems*, Communications in Numerical Methods in Engineering, **10**, 879–893, 1994.

18. P. KOWALCZYK, *Design optimization of cementless femoral hip prostheses using finite element analysis*, Transactions of the ASME, Journal of Biomechanical Engineering, **123**, 396–402, 2001.

19. P. KOWALCZYK, *Parameterized elastic properties of cancellous bone derived from finite element models of microstructure cells*, Submitted to Journal of Biomechanics, **36**, 961–972, 2003.

20. J. H. KUIPER, R. HUISKES, *Mathematical optimization of elastic properties: Application to cementless hip stem design*, Transactions of the ASME, Journal of Biomechanical Engineering, **119**, 166–174, 1997.

21. M. MARTENS, R. VAN AUDEKERCKE, P. DELPORT, P. DE MEESTER, J. C. MULIER, *The mechanical characteristics of cancellous bone at the upper femoral region*, Journal of Biomechanics, **16**, 971–983, 1983.

22. R. M. PILLIAR, J. M. LEE, C. MANIATOPOULOS, *Observation on the effect of movement on bone ingrowth into porous-surfaced implants*, Clinical Orthopaedics and Related Research, **208**, 108–113, 1986.

23. P. J. PRENDERGAST, *Finite element models in tissue mechanics and orthopaedic implant design*, Clinical Biomechanics, **12**, 343–366, 1997.

24. D. T. REILLY, A. H. BURSTEIN, *The elastic and ultimate properties of compact bone tissue*, Journal of Biomechanics, **8**, 393–405, 1975.

25. J. C. RICE, S. C. COWIN, J. A. BOWMAN, *On the dependence of the elasticity and strength of cancellous bone on apparent density*, Journal of Biomechanics, **21**, 155–168, 1988.

26. B. VAN RIETBERGEN, H. WEINANS, R. HUISKES, A. ODGAARD, *A new method to determine trabecular bone elastic properties and loading using micromechanical finite-element models*, Journal of Biomechanics, **28**, 69–81, 1995.

27. B. VAN RIETBERGEN, A. ODGAARD, J. KABEL, R. HUISKES, *Relationships between bone morphology and bone elastic properties can be accurately quantified using high-resolution computer reconstructions*, Journal of Orthopaedic Research, **16**, 23–28, 1998.

28. K. SCHITTKOWSKI, *NLQPL: A Fortran subroutine solving constrained nonlinear programming problems*, Annals of Operations Research, **5**, 1986, 485–500, 1986.

29. S. TOKARZEWSKI, J. J. TELEGA, A. GAŁKA, *A contribution to evaluation of effective moduli of trabecular bone with rod-like microstructure*, Journal of Theoretical and Applied Mechanics, **37**, 707–728, 1999.

30. C. H. TURNER, J. RHO, Y. TAKANO, T. Y. TSUI, G. M. PHARR, *The elastic properties of trabecular and cortical bone tissues are similar: results from two microscopic measurement techniques*, Journal of Biomechanics, **32**, 437–441, 1999.

31. D. Ulrich, B. van Rietbergen, A. Laib, P. Rüegsegger, *The ability of three-dimensional structural indices to reflect mechanical aspects of trabecular bone.* Bone, **25**, 55–60, 1999.

32. R. J. Yang, K. K. Choi, R. D. Crowninshield, R. A. Brand, *Design sensitivity analysis: a new method for implant design and a comparison with parametric finite element analysis*, Journal of Biomechanics, **17**, 849–854, 1984.

33. H. S. Yoon, J. L. Katz, *Ultrasonic wave propagation in human cortical bone. II. Measurement of elastic properties and micro-hardness*, Journal of Biomechanics, **9**, 459–464, 1976.

34. O. C. Zienkiewicz, *The finite element method*, McGraw–Hill, 1977.

Received September 30, 2002.